REPORT DOCUMENTATION PAGE

Form Approved OMB NO. 0704-0188

1. REPORT DATE (DD-MM-YYYY)	2. REPORT TYPE	3. DATES COVERED (From - To)
	New Reprint	-

4. TITLE AND SUBTITLE

Atomic scale mixing for inertial confinement fusion associated hydro instabilities

5a. CONTRACT NUMBER	5b. GRANT NUMBER	5c. PROGRAM ELEMENT NUMBER	5d. PROJECT NUMBER	5e. TASK NUMBER	5f. WORK UNIT NUMBER
W911NF-09-1-0306		611102			

6. AUTHORS

J. Melvin, P. Rao, R. Kaufman, H. Lim, Y. Yu, J. Glimm, D.H. Sharp

7. PERFORMING ORGANIZATION NAMES AND ADDRESSES

Research Foundation of SUNY at Stony Brc
Office of Sponsored Programs
W-5510 Melville Library
Stony Brook, NY 11794 -3362

8. PERFORMING ORGANIZATION REPORT NUMBER

9. SPONSORING/MONITORING AGENCY NAME(S) AND ADDRESS (ES)

U.S. Army Research Office
P.O. Box 12211
Research Triangle Park, NC 27709-2211

10. SPONSOR/MONITOR'S ACRONYM(S)
ARO

11. SPONSOR/MONITOR'S REPORT NUMBER(S)
54161-MA.43

12. DISTRIBUTION AVAILIBILITY STATEMENT

Approved for public release; distribution is unlimited.

13. SUPPLEMENTARY NOTES

The views, opinions and/or findings contained in this report are those of the author(s) and should not contrued as an official Department of the Army position, policy or decision, unless so designated by other documentation.

14. ABSTRACT

Hydro instabilities have been identified as a potential cause of performance degradation in inertial confinement fusion (ICF) experiments. We study instabilities associated with a single Richtmyer eMeshkov (RM) interface in a circular geometry, idealized from an ICF geometry. In an ICF application, atomic level mix, as an input to nuclear burn, is an important, but difficult to compute, variable. We find numerical convergence for this important quantity, in a purely hydro study, with only a mild dependence on the Reynolds number of the flow, in the high Reynolds number limit. We also find that

15. SUBJECT TERMS

Hydro instabilities, Inertial confinement fusion

16. SECURITY CLASSIFICATION OF:			17. LIMITATION OF ABSTRACT	15. NUMBER OF PAGES	19a. NAME OF RESPONSIBLE PERSON
a. REPORT	b. ABSTRACT	c. THIS PAGE			James Glimm
UU	UU	UU	UU		19b. TELEPHONE NUMBER 631-632-8370

Report Title

Atomic scale mixing for inertial confinement fusion associated hydro instabilities

ABSTRACT

Hydro instabilities have been identified as a potential cause of performance degradation in inertial confinement fusion (ICF) experiments. We study instabilities associated with a single Richtmyer eMeshkov (RM) interface in a circular geometry, idealized from an ICF geometry. In an ICF application, atomic level mix, as an input to nuclear burn, is an important, but difficult to compute, variable. We find numerical convergence for this important quantity, in a purely hydro study, with only a mild dependence on the Reynolds number of the flow, in the high Reynolds number limit. We also find that mixing properties show a strong sensitivity to turbulent transport parameters; this sensitivity translates into an algorithmic dependence and a nonuniqueness of solutions for nominally converged solutions. It is thus a complication to any verification and validation program. To resolve the nonuniqueness of the solution, we propose a validation program with an extrapolation component, linking turbulent transport quantities in experimental regimes to mildly perturbed turbulent transport values in ICF Reynolds number regimes. In view of the observed solution nonuniqueness, the validation program and its justification from the results presented here, has a fundamental significance.

REPORT DOCUMENTATION PAGE (SF298)
(Continuation Sheet)

Continuation for Block 13

ARO Report Number 54161.43-MA
Atomic scale mixing for inertial confinement fusi...

Block 13: Supplementary Note

Approved for public release; distribution is unlimited.

High Energy Density Physics 9 (2013) 288–296

Contents lists available at SciVerse ScienceDirect

High Energy Density Physics

journal homepage: www.elsevier.com/locate/hedp

Atomic scale mixing for inertial confinement fusion associated hydro instabilities

J. Melvin [a,*], P. Rao [a], R. Kaufman [a], H. Lim [a], Y. Yu [a], J. Glimm [a], D.H. Sharp [b]

[a] Department of Applied Mathematics and Statistics, Stony Brook University, Stony Brook, NY 11794-3600, USA
[b] Los Alamos National Laboratory, Los Alamos, NM 87545, USA

ARTICLE INFO

Article history:
Received 31 May 2012
Received in revised form
9 November 2012
Accepted 8 January 2013
Available online 26 January 2013

Keywords:
Hydro instabilities
Inertial confinement fusion

ABSTRACT

Hydro instabilities have been identified as a potential cause of performance degradation in inertial confinement fusion (ICF) experiments. We study instabilities associated with a single Richtmyer–Meshkov (RM) interface in a circular geometry, idealized from an ICF geometry. In an ICF application, atomic level mix, as an input to nuclear burn, is an important, but difficult to compute, variable. We find numerical convergence for this important quantity, in a purely hydro study, with only a mild dependence on the Reynolds number of the flow, in the high Reynolds number limit. We also find that mixing properties show a strong sensitivity to turbulent transport parameters; this sensitivity translates into an algorithmic dependence and a nonuniqueness of solutions for nominally converged solutions. It is thus a complication to any verification and validation program. To resolve the nonuniqueness of the solution, we propose a validation program with an extrapolation component, linking turbulent transport quantities in experimental regimes to mildly perturbed turbulent transport values in ICF Reynolds number regimes. In view of the observed solution nonuniqueness, the validation program and its justification from the results presented here, has a fundamental significance.

1. Introduction

1.1. Background

Hydro instabilities are known to limit inertial confinement fusion (ICF) neutron production [1]. See also the more recent discussions in Ref. [2]. For predictions of neutron production, the atomic level description of temperature and mixture concentrations provide the main input to a thermonuclear (TN) burn computation [3]. The interest in mix is brought about by current experiments of ICF processes. For instance, there is an observed degradation of 40–75% in neutron production, attributed to atomic mixing, estimated [4] based on experiments conducted on the Omega laser. In addition, it is proposed that low mixing is required to achieve ignition, specifically, the required maximum level of contaminated fuel from the ablator material must be less than an estimated 25%–40% [1]. Modal growth factors of 10–100 or more are reported in the linearized analysis of [1], suggesting a role for the nonlinear mode coupling and even perhaps the fully developed turbulent mixing regimes, beyond the ablation stabilized weakly nonlinear theory reviewed in Ref. [5]. ICF simulations do not predict correctly the observed dynamics of ICF capsules, which exhibit significant yield degradation relative to design. Thus a re-examination of the validation process would appear to be appropriate. Experimental analysis [6] of the ICF hot spot mix is based on Ge doped ablator material found within the hot spot at ignition time. Only mix at a level as predicted by design analysis was observed.

Known ICF instabilities or asymmetries occur primarily in four distinct stages during an ICF process. They begin with (1) the laser drive and are followed by (2) instability growth at the ablation surface. In addition, (3) Richtmyer–Meshkov (RM) instabilities occur at the boundary of ablator to deuterium-tritium (DT) ice and the boundary of DT ice to DT gas. These propagate inward to define initial conditions for the (4) deceleration phase, which is known to be strongly RT unstable. The second of these instabilities is an ablation modified RT instability, the third is RM and the fourth is RT in nature. In Ref. [7], velocity perturbations of 1% at the beginning of the deceleration phase (4) are considered to be dangerous for the performance of the capsule. The Verification and Validation (V&V) methods of this paper are applicable to the second, third and fourth instabilities mentioned above. Inaccuracies in prediction of the yield cliff suggests a possible need for improved modeling of the ablation phase, such as the inclusion of subgrid scale (SGS) models as proposed in Ref. [2], and the value in reexamination of any of the four instability stages, as well as other issues not discussed here.

* Corresponding author.
E-mail addresses: jmelvin@ams.sunysb.edu (J. Melvin), glimm@ams.sunysb.edu (J. Glimm).

1574-1818/$ – see front matter © 2013 Elsevier B.V. All rights reserved.
http://dx.doi.org/10.1016/j.hedp.2013.01.007

Here we address V&V aspects of a hydro instability study related to these broad ICF concerns. We study the RM instability, which is a primary ICF hydro instability, in its relation to atomic scale mix; the conclusions have implications for RT V&V as well.

The main thrust of the paper is to offer scientific data in support of a proposal for validation with extrapolation. We use a single code with no free parameters, validated in common for RT and RM data. This goal, infeasible for Reynolds Averaged Navier–Stokes (RANS), is a natural objective for Large Eddy Simulations (LES), which use dynamic SGS models. Validation for RT was previously considered and is summarized in Sec. 1.4. The RT case is more sensitive to transport (molecular, turbulent or numerical) than are RM instabilities. RT is thus more demanding for validation. This difficulty can be inferred from the fact that (in the authors' opinion) the FT/LES/SGS code discussed here appears to be unique as a multimode RT validated compressible LES code. For RM, we rely on an extensive code comparison study [8] with RAGE [9]. Generally excellent agreement was found for most measures of comparison, however, exceptions were noted for the temperature field (resolved in favor of our code FronTier (FT)). In the case of high density ratios, such as those that occur at the hot/cold DT interface in an ICF capsule, the edges of the mixing zone showed slow numerical convergence, especially for RAGE, indicating potential problems for commonly used resolution levels. Translated into the ICF context, this raises the question of simulation velocity perturbations at the beginning of the deceleration phase and perhaps of penetration of cold DT gas from the original DT ice layer of an ICF capsule into the ICF hot spot, or of ablator material (as has been observed experimentally), any of which can potentially degrade performance. Here we are mainly concerned with the extrapolation from the experimental regime to an ICF regime or to still higher Reynolds numbers. For the purpose of this paper, we understand the experimental regime to be $Re \approx 3.5 \times 10^4$, typical of laboratory RT experiments and the ICF regime to be $Re \approx 6 \times 10^5$, with higher values of *Re* also considered. We observe that the obvious step of RT validation using NIF or Omega laser data does not address the multimode, mode coupling RT growth stage, as the laser experiments performed to date have not reached this time regime.

The two main steps suggested here (RT validation and assessment of high *Re* extrapolation, with a zero parameter, theoretically constrained model) are not part of common V&V methodology. Most multiphysics codes fail for RT validation in the LES regime, and generally ICF codes do not employ dynamic subgrid scale models, which allow for smooth extrapolation from experimental to ICF Reynolds numbers. The validation proposed here is suggested as a complement to, or preliminary to, and not a replacement for, validation as presently performed. The most fundamental validation (as yet apparently still an open question) is comparison of simulations against ICF capsule performance directly.

The issue we raise is that the atomic mix properties are sensitive to the turbulent transport coefficients, and through them to the numerical algorithm. Stated more directly, apparently converged solutions are nonunique. They depend in an essential manner on details of the numerical algorithm. This unfortunate fact is documented here. However, we find only a mild variation in these coefficients in passing from an experimental regime to the ICF regime, as far as purely hydro issues are concerned. Thus a mild extrapolation from experimentally validated transport coefficients is feasible, yielding a significant constraint on the turbulent transport terms. We bridge this gap using algorithmic choices supported and constrained by theory and mathematical verification. We propose a program to carry out this objective, based on (a) a numerical algorithm with front tracking, to limit numerical thermal conduction and concentration diffusion and on (b) dynamic subgrid models to assure a theoretically consistent parameter free setting of the turbulent transport coefficients.

The context of the present study is a circular Richtmyer–Meshkov fluid instability problem; in view of the twin computational requirements of extreme levels of mesh refinement and of a parametric variation study involving multiple simulations, we consider this problem in 2D. At high *Re*, with ionized molecules, we consider a fluid with plasma like properties. These particles may be strongly coupled to a radiation field, while the thermal conduction between ions may be mediated by the ion-electron thermal coupling and the faster electron thermal diffusion. To model at a purely hydro level, we assume a highly heat conductive Prandtl number $Pr = 10^{-4}$ and a Schmidt number $Sc = 1$. We define the high *Re* limit to be taken as viscosity $\nu \to 0$, with fixed values for *Sc* and *Pr*. The parameter study analyzes a series of mesh levels and *Re* values, up to $Re = 6 \times 10^7$ and $Re = \infty$, extending a study [10] of the same problem. In future work, we will include plasma and radiation effects.

1.2. Summary of main results

Here, we explain a fundamental V&V challenge and present scientific data which supports a V&V route to bypass these obstacles. The challenge is the nonuniqueness and algorithmic dependence of nominally converged solutions for turbulent mixing problems. The route to bypass this obstacle is the combined use of parameter free dynamic SGS models and control over numerical diffusion through front tracking.

To validate this algorithmic choice, we use a two step V&V method. The main step is RT validation against the wealth of RT experimental data at $Re \approx 3.5 \times 10^4$. This data is highly sensitive to transport (molecular, turbulent, numerical) to the point that the FT/LES/SGS code used here appears to be the unique compressible multiphysics LES code to have been validated in a zero parameter manner against this data. This first step was reported in earlier publications [11,12] and is summarized here.

The second step in our V&V method is an extrapolation from $Re \approx 3.5 \times 10^4$ to the ICF regime of $Re \approx 6 \times 10^5$ or higher up to $Re = \infty$. This step leads to the main technical result of this paper. In essence, we show (a) that the consequences of the extrapolation are not large in their influence on numerical simulations, and (b) that there is an available theory to constrain the extrapolation. The theory [13], which is the basis of dynamic SGS models, is not new to this paper.

Thus our main results can be stated as (a) numerical convergence of the turbulent mixing statistics in question and (b) a small magnitude of the perturbation in these statistics due to a change of *Re*.

1.3. The numerical algorithm

The numerical study is based on the front tracking code FronTier [14,15], enhanced with an LES turbulence model having dynamic SGS terms [13]. We refer to this algorithm as FT/LES/SGS. These two algorithms are built upon a hydro package (compressible, with general equation of state) using the MUSCL [16] algorithm. To facilitate coupling of these features with other hydro packages, we have developed an API. To avoid complications with multispecies diffusion [17], we assume mixing of two fluids only.

1.3.1. Front tracking

With front tracking, our aim is to achieve enhanced resolution of interfaces between fluids and maintain this resolution throughout the simulation. This allows us to minimize the numerical mass diffusion associated with steep concentration or thermal gradients. We see improved results even for coarser grids, since the discontinuity that normally leads to the smearing in coarser grids is

dynamically tracked, preventing one fluid from numerically interacting across the interface with the other.

We accomplish this goal by creating a separate, lower dimensional mesh along the front (interface) which separates the fluids, for example following an iso-temperature contour within a sharp thermal gradient. The front then separates fluids with distinct physical characteristics. During each time step we propagate the front's mesh to its new location based on the surrounding interior states. The front points are propagated in a normal direction, utilizing a Riemann problem formulation to resolve the different velocities obtained via one sided extrapolation from interior states to the front location.

When interfacial tangling occurs, we utilize algorithms to untangle and redistribute points on the front mesh, allowing for a logical reconstruction of a tangled interface. For more information on this process and the FronTier front tracking algorithm, we refer the reader to [15,18,19].

The front mesh is overlayed on a normal Eulerian grid. Where it intersects cells, we cut those cells into multiple pieces to ensure separation of the distinct fluids across an interface, illustrated in Fig. 1.

When updating interior states on a cut cell, ghost cells constructed from states defined in neighboring cells on the same side of the front allow for a 1-sided update, consisting only of states from those cells on the same side of the discontinuity interface.

This construction allows us to control numerical diffusion, especially with complicated interfaces, as arise in hydro instabilities in ICF processes.

1.3.2. LES with dynamic subgrid models

The purpose of subgrid models is to capture the effect of the unresolved scales (below the grid level) on those that are resolved. We start with the interpretation that the numerical solution values represent grid cell averaged quantities. Conventionally, in the derivation of filtered Navier–Stokes equations for use in Large Eddy Simulations, there is a convolution average by a positive weight function (the filter), and the equations are derived for the filtered quantities. We omit this filter step, and use the cell averaged quantities directly. The average of the nonlinear terms introduces new unknowns into the equations for which new equations, called closures, are required. These show up as flux type terms, and are the origin of the turbulent transport. The closure term must be modeled; often a solution gradient is used for a turbulent flux, with an undetermined coefficient. With dynamic subgrid models [13,20,21], the otherwise missing coefficient is determined by the numerical solution itself, and varies with space-time according to local flow conditions. The determination is achieved by consideration of the closure on the current grid and on a once coarser grid, and by an asymptotic assumption that the model coefficient is a mesh convergent or asymptotically mesh independent quantity, so that a common value can be used between the two grid levels considered. The advantage of cell averages as opposed to a filter is the absence of loss of spatial resolution and of solution fluctuations averaged over by the filter.

1.3.3. API

The API is presently under development http://www.ams.sunysb.edu/~rkaufman/api.

Presently, it links a client code to the FT/LES/SGS front tracking library. All functions in the API are designated as belonging to the API or to the client. Those belonging to the client depend on client specific information, such as the data layout of solution state values. For these functions, the API includes a reference implementation in a few regular cases, such as for regular rectangular grid based state data. The main point of the API functions is to communicate data between the client and the front library. This communication is, of course, two directional. From the client data, we extract velocities, used to advance the front in time. From the front library, we extract front location information, used in a client function to label any given finite difference stencil as regular or irregular, according to whether the stencil does not or does cross a tracked front. Finally, a client function will offer modified (tracked) stencil state values, to affect ghost cells in a neighborhood of the front. The modified stencil of state values will be differenced using the usual client difference algorithm.

1.4. Prior validation and code comparison studies for FT/LES/SGS

1.4.1. Rayleigh–Taylor

FT/LES/SGS has achieved systematic agreement with a wide range of Rayleigh–Taylor experiments, including mixing of both concentration and thermal fields. Uncertainty over initial conditions (not recorded) has been resolved, by backward solution of the fluid equations from an early time (recorded) to an initial time (not recorded), and with uncertainty quantification for the possible errors in the reconstruction [22]. Agreement is precise enough to distinguish between distinct experiments and their distinct values of α. See Table 1.

1.4.2. Richtmyer–Meshkov

FronTier was used in a three way code comparison (with RAGE and PROMETHEUS), with experiment and with theory [26] for single mode Richtmyer–Meshkov instabilities. Extensive comparison of FT/LES/SGS with the already validated RAGE code for multimode Richtmyer–Meshkov instabilities, before and after reshock, gave generally excellent results [8], with exceptions related to the

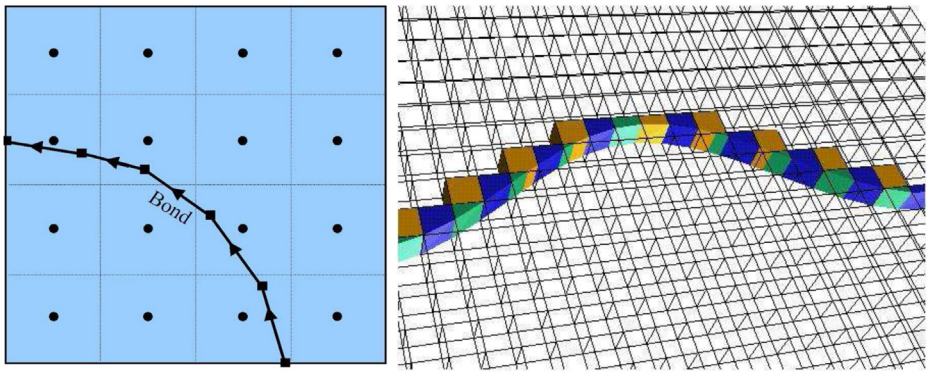

Fig. 1. Discretized interface and cut cell construction. Left: Tracked front overlayed over Eulerian grid, discretized at front points. Right: Display of cut cells created when an interface cuts through a cell.

Table 1
Experimental and FT/LES/SGS simulation values of α compared for a series of experiments, with error bars, if provided, by either the simulation or the experiment, and the discrepancy if any.

Experiment	α_{exp}	α_{sim}	Discrepancy
Smeeton–Youngs [23] #112	0.052	0.055	6%
Smeeton–Youngs [23] #105	0.072	0.072–0.080	0%
Smeeton–Youngs 10 exp.	0.055–0.077	0.066	0%
Andrews–Banerjee [24]	0.065–0.07	0.069	0%
Andrews–Muschke [25]	0.059–0.081	0.075	0%
Andrews–Muschke [25]	0.08–0.09	0.084	0%

thermal field as noted above. In view of the more difficult RT thermal validation and the absence of thermal RM experimental data, we plan to proceed to the next stage of our studies, which is to bring the simulations closer to an ICF experimental plane.

1.5. Outline of paper

In Sec. 2, we expand on a method for stochastic convergence of turbulent solutions we previously introduced and lay the framework for the convergence strategy of our algorithm. In Sec. 3, we study the convergence of the solution PDFs and their variation with *Re*. In Sec. 4, we show that the PDFs are sensitive to the definition of turbulent transport. In other words, we establish numerical non-uniqueness for turbulent mixing in the high *Re* limit. In Sec. 5 we outline our ideas for the validation of numerical studies of hydro instabilities related to ICF performance.

2. Stochastic convergence of turbulent solutions

2.1. Convergence analysis method

Our convergence strategy is stochastic in nature and it is algorithmically a post processing method. Therefore, it does not modify the simulation itself. The authors are not aware of a similar construction employed by others for analysis of numerical solutions of partial differential equations. We retain solution stochastic information (fluctuations and their PDFs) through a coarse graining strategy where we organize the mesh cells into a coarse grained mesh of supercells. All solution values in a single supercell are combined to form a finite approximation to a probability density function (PDF) or its indefinite integral, the cumulative distribution function (CDF). In this construction, the coarse grained supercell provides the (reduced) spatial or space-time localization. Such a construction is a discrete approximation to a space-time dependent probability measure, also known as a Young Measure. Whether assessing convergence or the effects of variation of physical parameters, we are comparing solutions. The difference between solutions is expressed, in each supercell, as the difference between two coarse grain localized CDFs. In each supercell, the solution data is discretized into bins based on the solution variables under study. From this binned data, we create an empirical PDF or CDF. The norm of the difference is defined first through an L_1 norm over the solution state variables, i.e., of the L_1 norm difference of the CDFs over the space of bins, and normalized by division by the number of bins, and by division by the difference between the maximum and minimum solution values over the domain. Such a norm difference is defined as a function defined on each supercell. A spatial mean (an L_1 norm over all supercells in the domain, divided by the total supercell area in the domain) completes the definition of the norm of the difference of the CDFs. This strategy for convergence has been developed in previous papers [11,27,28].

2.2. Supercell and bin sizing

We now examine choices for bin and supercell size. The main focus of this paper is on the distribution of temperature and concentration values. In this section, we focus on the concentration marginal PDF, as its convergence is more sensitive. A common model for concentration PDFs is the beta distribution, which we use as a surrogate to analyze supercell and bin selections.

For a mass fraction x, the beta distribution has a PDF $x^{\alpha-1}(1-x)^{\beta-1}/B(\alpha,\beta)$ with the normalizing constant $B(\alpha,\beta) = \int_0^1 u^{(\alpha-1)}(1-u)^{(\beta-1)}du$. This distribution is completely characterized by its mean μ and variance σ, related to α and β by the formulas $\alpha = (\mu^2-\mu^3-\mu\sigma^2)/\sigma^2$ and $\beta = (\mu-2\mu^2+\mu^3-\sigma^2+\mu\sigma^2)/\sigma^2$. In Fig. 2 left, we plot the histogram of all concentration values taken from the middle 80% of the mixing zone at $t = 90$, shortly after reshock, for $Re = 6 \times 10^7$. In this paper, we focus our analysis on the middle 80% of the mixing zone, in order to reduce the edge effects of the mixing zone. We determine the parameters $\alpha = 0.360$ and $\beta = 0.286$ from this data and plot the corresponding beta distribution PDF. In Fig. 2 right, we compare the empirical (solid curve) and theoretical (dotted curve) CDFs of these two distributions. The L_1 difference, an assessment of the model error, is 0.074.

The supercell size regulates the amount of stochastic information captured in this description and the level of spatial resolution lost in the process. In order to assess mesh convergence issues, we choose supercells large enough that the statistical errors are small relative to the mesh errors. Statistical sampling errors are typically $\mathcal{O}(n^{-1/2})$, where n is the number of cells in a supercell.

We begin with the model beta distribution, determined by the parameters specified above, and take repeated random samples of a fixed size. We analyze each individual sample, by binning the data

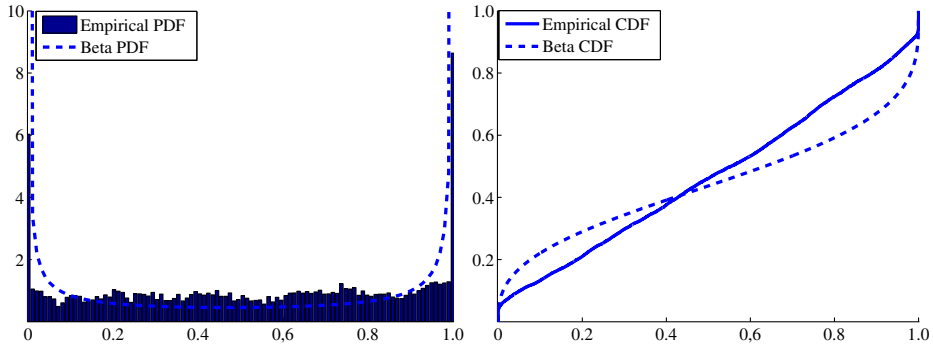

Fig. 2. Left. Histogram for concentration data and beta distribution with the parameters $\alpha = 0.360$, $\beta = 0.286$ (dotted curve). Data from $Re = 6 \times 10^7$ coarse grid (II) simulation, $t = 90$. Right. Empirical CDF of the data (solid curve) in middle 80% of the mixing zone from the same simulation as left and beta distribution CDF (dotted curve) with the same parameters α, β.

Table 2
Statistical convergence rates for repeated finite samples of fixed size drawn from the beta distribution, parameters as above. 10 Bins used to construct the CDFs.

Sample size	25	100	400	1600
Mean of L_1 norm error for CDFs	0.067	0.033	0.017	0.009
STD of L_1 norm error for CDFs	0.035	0.018	0.009	0.005

and forming a sample CDF from the sample data and then taking an L_1 norm between the sample CDF and the beta distribution itself. The L_1 norms are then averaged over the repeated samples to determine an expected mean statistical error that results from the supercell process. In Table 2, we display the means and the STDs of the statistical errors that arise for different sizing of supercells. We can see that upwards of 400 points per supercell are necessary to reduce the statistical error to a value less than 2%. This classifies the tradeoff between supercell sizing (spatial resolution) and accuracy (statistical error) of the method.

To verify the beta distribution as a model for the concentration data, we also repeat the sampling process using the empirical data from the coarse grid (II: 400×800) $Re = 6 \times 10^7$ simulation (used to calculate the beta distribution parameters). In the left frame of Fig. 3, we plot the average statistical errors found when comparing the beta distribution to finite samples drawn from it. In the right frame, we plot the average statistical errors found when comparing empirical CDFs of the raw data from the middle 80% of the mixing zone and random samples drawn from this data. Comparing the differences between the theoretical formulation and our specific application, we see roughly unchanged errors between the beta distribution and the empirical distribution, thus justifying the choice of the beta distribution as a surrogate for the concentration PDFs. We also show in Fig. 3 insensitivity of the statistical errors to bin size.

From the above analysis, we draw the following conclusions:

1. As a result of the insensitivity of the bin size parameter, we use a bin sizing of 10, per variable, in all analysis performed in this paper.
2. To obtain statistical errors significantly smaller than mesh errors, we choose to use a supercell size close to 400 data points in each supercell on the coarse grid (II: 400×800).

3. High Reynolds number asymptotics

Here we show, in a purely hydro context, the mildness of the variation introduced in passing from an experimental regime of $Re \approx 3.5 \times 10^4$, well studied experimentally for related Rayleigh–Taylor instabilities, to the ICF regime of $Re \approx 6 \times 10^5$ and larger.

Table 3
L_1 norm convergence of joint CDFs for temperature and concentration (central column) and concentration only (right column) for an RM instability with $Re = 6 \times 10^7$. Meshes: I 200×400, II 400×800, III 800×1600, IV 1600×3200.

Mesh	Temp and conc	Conc
I–IV	0.092	0.124
II–IV	0.064	0.079
III–IV	0.045	0.058

This fact supports our V&V proposal of experimental validation at $Re \approx 3.5 \times 10^4$ with verification extrapolation to $Re \approx 6 \times 10^5$.

3.1. Convergence of joint temperature–concentration PDFs

We begin by analyzing the convergence properties of the joint temperature–concentration CDFs within the middle 80% of the mixing zone for the $Re = 6 \times 10^7$ simulation. L_1 norm convergence of the joint temperature–concentration CDFs was established in Ref. [10] for lower Re values, so this value for Re represents an extension of the convergence regime as well as an extension to the case $Pr = 10^{-4}$.

For the supercell gridding, since our mixing zone is radial, we use supercells in r, θ space. Since the data is homogeneous in the θ direction and sensitive to the r direction, discussed in further detail in Sec. 3.2, we use 10 supercells in the radial direction and 2 supercells in the angular direction, with a domain consisting only of the data points contained in the common mixing zone. With the data structured in x, y space, the r, θ bins have an unequal number of points, with an average of 642 points within each supercell of the coarse grid (II: 400×800). The results of this analysis are presented in Table 3, from which we see evidence of norm convergence for the CDFs under mesh refinement. The slow convergence rate observed here is consistent with the results of [10], which used an alternate convergence analysis method.

We investigate the dependence of the convergence analysis on the supercell griddings in Table 4. We compare an 8×1 (8 in r, 1 in θ), 16×2, 32×4 and 64×8 supercell grid structure. As the region contained within a supercell increases (the number of points within a supercell increases, such as moving from 64×8 towards 8×1), the average norm error decreases. The average number of points in a supercell on the coarse grid is approximately 1600, 400, 100 or 25, respectively. We attribute the increase in the norm error to the statistical errors found in Sec. 2.2. Consistent with this interpretation is the fact that the increase of error with supercell size is nearly independent of the computational rows. We also note that the slight difference between the 1×1 and 1×8 supercell gridding is due to the convergence of the statistical errors, within

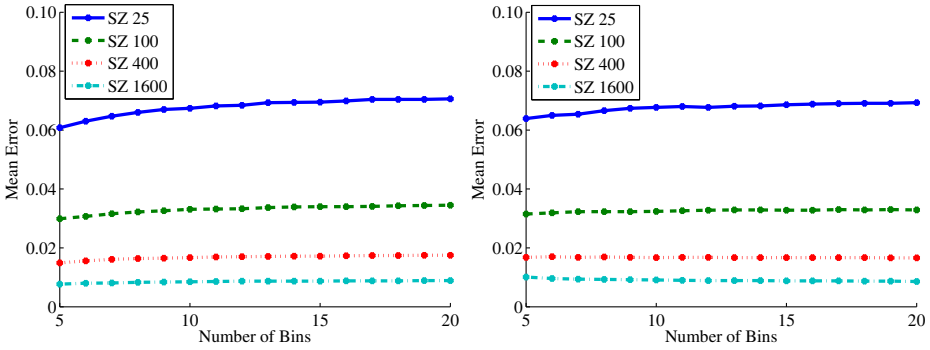

Fig. 3. L_1 norm of the differences of the concentration CDFs. Left: Repeated finite samples of fixed size, drawn from the beta distribution. Right: The empirical CDF from raw data in the middle 80% of the mixing zone and repeated random samples from this data. The four sample sizes plotted are: 25, 100, 400 and 1600.

Table 4
Variation in the L_1 norm comparison of joint CDFs across mesh levels for different choices of supercells. A coarser supercell mesh corresponds to larger supercells, and improved statistical convergence. All supercell choices are given in radial × angular direction. Meshes as above.

Supercell grid	1 × 1	8 × 1	16 × 2	32 × 4	64 × 8
I–IV	0.079	0.085	0.094	0.102	0.138
II–IV	0.057	0.059	0.065	0.080	0.103
III–IV	0.039	0.041	0.047	0.059	0.076

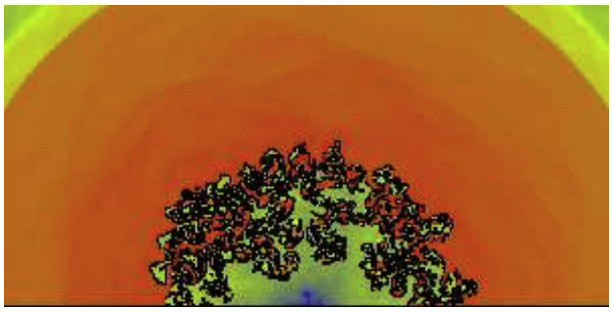

Fig. 4. Density plot for $Re = 6 \times 10^7$ after reshock.

a fraction of a percentage point. The supercell size (10 × 2) selected is a tradeoff between statistical accuracy and spatial resolution.

3.2. Spatial variation of mix

In Fig. 4, we plot the density over the mixing zone after reshock, for $Re = 6 \times 10^7$.

The statistics of the PDFs, as they depend on x, y or r, θ, appear uniform in θ but the edge regions for r differ from the central region. The unmixed light fluid (in the mixing zone) is preferentially located near the inner edge and the unmixed heavy fluid is similarly noticeable near the outer edge of the mixing zone.

For $Re = \infty$, we plot the PDFs in four separate zones for the r values, with two central zones and two edge zones, see Fig. 5. We observe radial dependence in the mixing properties, with edge zone PDFs containing substantial amounts of unmixed fluids. The outer region has significant unmixed heavy fluid and the inner region significant unmixed light fluid. The central zones, especially the outer central zone, are nearly equiprobable in their distribution, meaning that any mixture fraction is approximately as probable as any other. The inner central zone and the inner edge zone also have significant unmixed light fluid concentrations.

We conclude that the temperature and concentration fluctuations are essentially stationary statistically in θ and nearly so in r except near the mixing zone edges. We choose supercells aligned with r, θ coordinate boundaries, large (a) in view of the near stationarity of the statistics and (b) in view of the desire to observe convergence under mesh refinement, and thus to reduce the statistical sampling errors relative to the mesh errors. As with any convergence issue, the resolution will improve as the mesh is refined. Our intention is to use stochastic convergence for assessing TN burn. TN burn is also a stochastic variable, but the available observations are somewhat coarse grained, and appear to be not greatly more refined than the supercells in use here.

3.3. Re dependence of mix

As a main result of this section, we display in Fig. 6, the joint PDFs of temperature and concentration for the medium grid (III: 800 × 1600) $Re = 3.5 \times 10^4$ and for $Re = 6 \times 10^7$. Visually there is minimal difference between the left frame, the experimental regime with Reynolds numbers of 3.5×10^4 and the right frame,

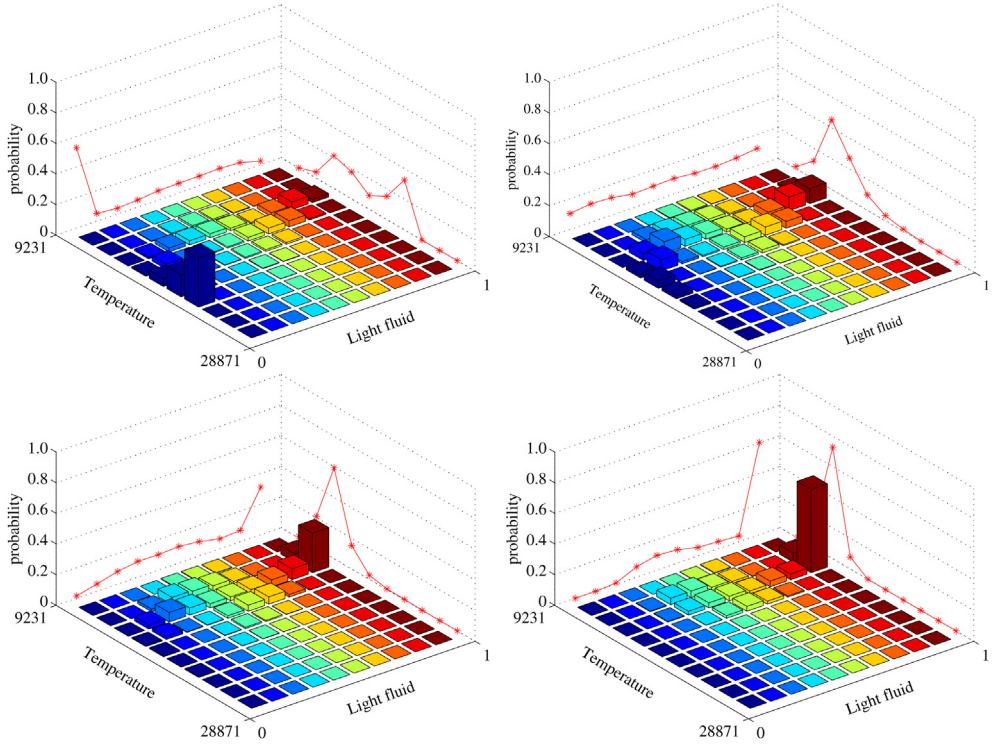

Fig. 5. PDFs for concentration and temperature for Reynolds number $Re = \infty$ with the variation of PDFs with the radius. Top row, left to right, outer edge r values, and outer central region. Bottom row, left to right, inner central region for r and inner edge region.

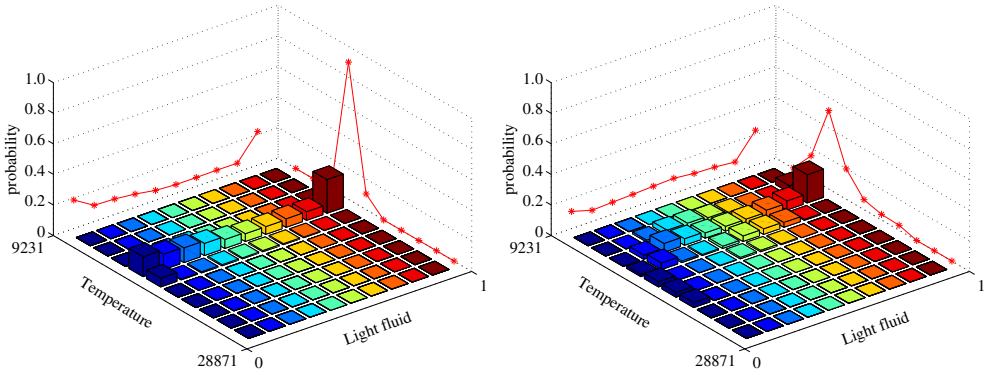

Fig. 6. Change of *Re*, $Re = 3.5 \times 10^4$ compared to $Re = 6 \times 10^7$. Left: Joint PDF of temperature and concentration at $Re = 3.5 \times 10^4$. Right: Joint PDF of temperature and concentration at $Re = 6 \times 10^7$.

Fig. 7. L_1 norm CDF differences between Fig. 6, left, and right. The L_1 norms result from binning onto supercells, to achieve numerical approximation of the associated CDFs.

beyond the ICF Reynolds number of 6×10^5. We use a supercell grid of 10×2 as above, (approximately 642 points within coarse grid supercell), and consider only the concentration marginals. The *Re* related CDF norm difference of 0.077 is 1.3 times the mesh error of 0.058 (grids III–IV) and thus only marginally observable. See Fig. 7.

4. PDF sensitivity: an $n + 1$-parameter family of high *Re* limits

The n-species compressible Navier–Stokes equations, in the high *Re* limit, eliminates *Re* as a parameter. There remain $n + 1$ dimensionless fluid transport parameters. The $n - 1$ independent Schmidt numbers, the Prandtl number, and the ratio of two independent viscosities remain to characterize solutions of the Euler equations achieved in the high *Re* limit process. For LES it is expected that the limit $Re \to \infty$ is independent of the choice of physical transport parameters, if these are fixed and independent of *Re* in the infinite *Re* limit process. In this sense the limit is universal relative to molecular fluid transport.

The high *Re* limit, however, is sensitive to the path taken in the space of dimensionless total (turbulent and molecular) transport coefficients, if these coefficients are given *Re* dependent values. We demonstrate here sensitivity of the high *Re* limit to the dimensionless turbulent transport (SGS) terms and their coefficients. For high *Re* flows, all turbulent Schmidt numbers and the Prandtl number should coincide. There is one parameter to set this common value, which is constrained by validation, i.e., comparison to experiment. A second parameter is the ratio of bulk to shear turbulent viscosities. This important point of solution sensitivity arises in practice as dependence of the solutions upon the algorithms in the high *Re* limit. The algorithmic dependence of the solution underscores the importance of validation and the relevance within the experimental range of *Re*, and a mild *Re* dependent and theoretically based extrapolation, as far as pure hydro issues are concerned, for *Re* values beyond this range.

From this discussion, we see the importance of turbulence models. A similar discussion (not included here) would show the importance of initial/boundary conditions or forcing functions. If explicit SGS terms are not used, then the fixed point is sensitive to algorithmic details. If a numerical algorithm has significant

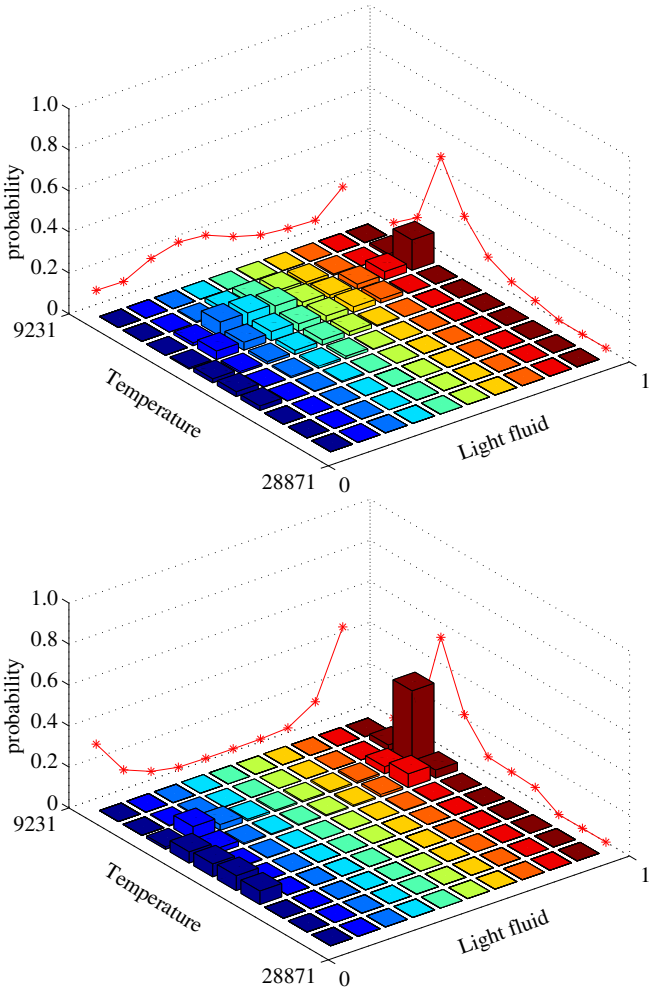

Fig. 8. PDFs for the joint concentration–temperature distribution for two values of the turbulent transport coefficient for concentration diffusion. Above: 10 times nominal and below: 0.1 times nominal. $Re = 6 \times 10^7$.

numerical diffusion (e.g., if tracking is not used), then algorithmic issues will affect the fixed point even if SGS terms are included. Diffusion, once added numerically, cannot be removed through addition of SGS terms. Thus, we anticipate that numerical algorithms with significant species concentration diffusion will reach only a fraction of the full $n + 1$ dimensional parameter space of high *Re* limits. Mesh refinement short of a DNS simulation will not change this statement.

We justify the assertion of solution nonuniqueness by showing that modifications to the dimensionless turbulent mass diffusion up or down by factors of 10 change the PDFs of the solution variables. We plot in Fig. 8, the joint PDFs for concentration and temperature, after an increase and a decrease of turbulent concentration diffusion by factors of 10. We see that the high *Re* solution is sensitive to the choice of turbulence model. Comparing spatially dependent CDFs obtained by binning solution values into supercells, we find an L_1 norm difference of 0.187 between these two simulations, when using a 10×2 supercell grid and analyzing only the concentration marginal. This L_1 norm difference value is more than three times as large as the mesh error difference for this grid resolution and more than double the normed difference between the simulations with $Re = 3.5 \times 10^4$ compared to $Re = 6 \times 10^7$, presented in Sec. 3.3. Thus we conclude that the differences in turbulent mass diffusion are significant and observable, in that they yield CDF differences 3.2 times larger than the statistical and mesh errors.

5. Conclusions

The results presented here are a demonstration, within the present research framework, that in the high *Re* limit of turbulent mixing, atomic mixing properties are sensitive to models for turbulent transport, and specifically to the numerical algorithm. The limit is demonstrated to be nonunique, supporting the idea that there is an $n + 1$-parameter family of fixed points for n-species mixing, with the fixed points labeled by the turbulence model or by the numerical algorithm. Among these nonunique choices, the FT/LES/SGS algorithm selects a unique limit, which agrees well with experiment within the experimental range of *Re*, in contrast to most ILES simulations, which do not [29]. The turbulent transport coefficients, within this dynamic SGS method, are uniquely specified by theory; the simulations have no tunable parameters. Since zero-parameter numerical models of complex physical phenomena (i.e. fluid turbulence and mixing in the present context) are not so common, we emphasize this aspect of the FT/LES/SGS algorithm. The algorithm is, in the opinion of the authors, unique among compressible LES simulations in its level of validation (experimental confirmation) for RT experiments. Because of the sensitivity of the atomic level mixture to turbulence models and numerical algorithms, experimental validation is important.

A major conclusion of the present paper is that the ICF regime of perhaps $Re \approx 6 \times 10^5$ is only a mild perturbation (in terms of strictly hydro issues) of an experimental regime of $Re \approx 3.5 \times 10^4$, for which there are numerous hydro instability experiments.

The main purpose of this paper is to establish scientific results which support a two step route with experiment and theory supported extrapolation to V&V for ICF simulations.

The method is suitable to the three main instability stages (ablation, RM interface instabilities and RT deceleration) of ICF. We explain the main difficulty (nonuniqueness of solutions) and its resolution (dynamic SGS models for LES and front tracking). We review previous work on the experimental comparison step and we present new material relating to the extrapolation step.

In future work, we will examine this strategy in simulations more closely modeling ICF. In essence, our proposal is that ICF hydro codes should be tested (validated) in the experimental regime and tested numerically (verified) for a parameter free extrapolation from there to the ICF regime and beyond. Initial conditions for the experimental regime are generally not known, but we have shown that these can be reconstructed from the early time data, with reconstruction uncertainty quantified and an overall effect of $\pm 5\%$ on the value of the RT growth rate α [22].

This is not the first time in which nonuniqueness has been an essential feature of the solutions of time dependent equations, modeled at the inviscid (Euler equation) level. Shock refraction problems, which describe self similar time dependent solutions, sometimes have multiple solutions. Flame speed is ambiguous when analyzed at the level of the Euler equations, with the ambiguity removed by consideration of the Prandtl number. Detonation waves allow multiple solutions, as weak or strong detonations [30], while some dissipative mechanism often selects the weak detonation. Equations suggested by three phase flow for petroleum reservoirs show nonuniqueness for wave interaction (Riemann) problems [31].

Within the study of turbulence, the sensitivity of solutions to turbulence models is widely understood. However, for turbulence modeling, the analogous resolution of ambiguity (specification of transport coefficients) requires specifying the turbulent transport, exactly the quantity which introduces the ambiguity.

Here we come to the conundrum which is the central theme of this paper. Nonuniqueness of solutions is removed by specification of turbulent (not laminar) transport coefficients, quantities not accessible to direct measurement in a nearly infinite Reynolds number regime, and regarding which there is substantial disagreement. The dynamic subgrid models provide a zero parameter solution. In other words they do select all needed coefficients, and remove all ambiguity. The dynamic subgrid models, combined with front tracking provide excellent agreement with experimental RT data (validation). Here we claim that validation followed by a mild perturbative verification step reaches the ICF regime. In view of the importance of this claim, we believe it should be subject to further testing and studies, a task we hope to carry out in the future.

Acknowledgments

This work is supported in part by the Nuclear Energy University Program of the Department of Energy, project NEUP-09–349, Battelle Energy Alliance LLC 00088495 (subaward with DOE as prime sponsor), Leland Stanford Junior University 2175022040367A (subaward with DOE as prime sponsor), Army Research Office W911NF0910306. Computational resources were provided by the Stony Brook Galaxy cluster and the Stony Brook/BNL New York Blue Gene/L IBM machine. This research used resources of the Argonne Leadership Computing Facility at Argonne National Laboratory, which is supported by the Office of Science of the U.S. Department of Energy under contract DE-AC02-06CH11357. David H. Sharp, Los Alamos National Laboratory, retired. We also thank the reviewers for their helpful comments and suggestions. Los Alamos National Laboratory preprint LA-UR-12–23768. Stony Brook University preprint SUNYSB-AMS-12–01.

References

[1] S.W. Haan, et al., Point design targets, specifications, and requirements for the 2010 ignition campaign on the national ignition facility, Phys. Plasmas 18 (2011) 051001.
[2] W. Goldstein, R. Rosner, Workshop on the Science of Fusion Ignition on NIF, Technical Report LLNL-TR-570412, LLNL, 2012.
[3] G. Caughlan, W. Fowler, Thermonuclear reaction rates V, At. Data Nucl. Data Tables 40 (1988) 283–334.

[4] D.C. Wilson, P.S. Ebey, T.C. Sangater, W.T. Shmayda, V.Y. Glebov, R.A. Lerche, Atomic mix in directly driven inertial confinement implosions, Phys. Plasmas 18 (2011) 112707.
[5] J.D. Lindl, P. Amendt, R.L. Berger, S.G. Glendinning, S.H. Glazer, S.H. Haan, R.L. Kauffman, O.L. Linden, L.J. Suter, The physics basis for ignition using indirect-drive targets on the national ignition facility, Phys. Plasmas 11 (2004) 339–491.
[6] S.P. Regan, R. Epstein, B.A. Hammel, L.J. Suter, J. Ralph, et al., Hot-spot mix in ignition-scale implosions on the NIF, Phys. Plasmas 19 (2012) 056307.
[7] S. Pfalzner, An Introduction to Inertial Confinement Fusion, Taylor and Francis, 2006.
[8] T.O. Masser, Breaking Temperature Equilibrium in Mixed Cell Hydrodynamics, Ph.D. thesis, State University of New York at Stony Brook, 2007.
[9] M. Gittings, R. Weaver, M. Clover, T. Betlach, N. Byrne, R. Coker, E. Dendy, R. Hueckstaedt, K. New, W.R. Oakes, D. Ranta, R. Stefan, The RAGE radiation-hydrodynamic code, Comput. Sci Discovery 1 (2008) 015005.
[10] H. Lim, Y. Yu, J. Glimm, X.L. Li, D.H. Sharp, Subgrid models for mass and thermal diffusion in turbulent mixing, Physica Scripta T142 (2010) 014062. Brook Preprint SUNYSB-AMS-08-07 and Los Alamos National Laboratory Preprint LA-UR 08–07725.
[11] T. Kaman, R. Kaufman, J. Glimm, D.H. Sharp, Quantification for turbulent mixing flows: Rayleigh–Taylor instability, in: A. Dienstfrey, R. Boisvert (Eds.), Book Quantification in Scientific Computing, Volume 377 of *SeriesIFIP Advances in Information and Communication Technology*, Springer, 2012, pp. 212–225. Stony Brook University Preprint number SUNYSB-AMS-11-08.
[12] T. Kaman, J. Glimm, D.H. Sharp, Uncertainty quantification for turbulent mixing simulation, in: 5th International Conference of Numerical Modeling of Space Plasma Flows (ASTRONUM 2010), Stony Brook University Preprint number SUNYSB-AMS-10-04, Los Alamos National Laboratory preprint LA-UR 11–00422, 444, 2010, p. 21.
[13] P. Moin, K. Squires, W. Cabot, S. Lee, A dynamic subgrid-scale model for compressible turbulence and scalar transport, Phys. Fluids A 3 (1991) 2746–2757.
[14] E. George, J. Glimm, J.W. Grove, X.-L. Li, Y.-J. Liu, Z.-L. Xu, N. Zhao, Simplification, conservation and adaptivity in the front tracking method, in: T. Hou, E. Tadmor (Eds.), Hyperbolic Problems: Theory, Numerics, Applications, Springer Verlag, Berlin and New York, 2003, pp. 175–184.
[15] W. Bo, X. Liu, J. Glimm, X. Li, A robust front tracking method: verification and application to simulation of the primary breakup of a liquid jet, SIAM J. Sci. Comput. 33 (2011) 1505–1524.
[16] P. Colella, A direct Eulerian MUSCL scheme for gas dynamics, SIAM J. Sci. Comput. 6 (1985) 104–117.
[17] R. Bird, W. Stewart, E. Lightfoot, Transport Phenomena Second Edition, John Wiley & Sons, New York, 2002.
[18] J. Glimm, J.W. Grove, Y. Zhang, Interface tracking for axisymmetric flows, SIAM J. Sci. Comput. 24 (2002) 208–236. LANL report No. LA-UR-01-448.
[19] J. Du, B. Fix, J. Glimm, X. Jia, X. Li, Y. Li, L. Wu, A simple package for front tracking, J. Comput. Phys. (2006) 613–628.
[20] M. Germano, U. Piomelli, P. Moin, W.H. Cabot, A dynamic subgrid scale eddy viscosity model, Phys. Fluids A 3 (1991) 1760–1765.
[21] T. Ma, Large Eddy Simulation Of Variable Density Flows, Ph.D. thesis, University of Maryland, 2006.
[22] J. Glimm, D.H. Sharp, T. Kaman, H. Lim, New directions for Rayleigh–Taylor mixing, Phil. Trans. Royal Soc. A: turbulent mixing and beyond, Los Alamos National Laboratory Preprint LA-UR 11-00423 and Stony Brook University Preprint SUNYSB-AMS-11-01, in press.
[23] V.S. Smeeton, D.L. Youngs, Experimental Investigation of Turbulent Mixing by Rayleigh–taylor Instability (Part 3). AWE Report Number 35/87 (1987).
[24] A. Banerjee, M.J. Andrews, Statistically steady measurements of Rayleigh–Taylor mixing in a gas channel, Phys. Fluids 18 (2006). 1994.
[25] N. Mueschke, O. Schilling, Investigation of Rayleigh–Taylor turbulence and mixing using direct numerical simulation with experimentally measured initial conditions. I. Comparison to experimental data, Phys. Fluids 21 (2009). 014106 1–19.
[26] R.L. Holmes, B. Fryxell, M. Gittings, J.W. Grove, G. Dimonte, M. Schneider, D.H. Sharp, A. Velikovich, R.P. Weaver, Q. Zhang, Richtmyer–Meshkov instability growth: experiment, simulation, and theory, J. Fluid Mech. 389 (1999) 55–79. LA-UR-97-2606.
[27] T. Kaman, J. Melvin, P. Rao, R. Kaufman, H. Lim, Y. Yu, J. Glimm, D.H. Sharp, Recent progress in turbulent mixing, Physica Scripta, Stony Brook University Preprint number SUNYSB-AMS-11-09, Los Alamos National Laboratory Preprint LA-ur 11–06770, in press.
[28] R. Kaufman, T. Kaman, Y. Yu, J. Glimm, Stochastic convergence and the software tool W*, in: Numerical Methods for Hyperbolic Equations: Theory and Applications, 2012, CRC, Taylor and Francis Group, Stony Brook University Preprint number SUNYSB-AMS-11-10.
[29] G. Dimonte, D.L. Youngs, A. Dimits, S. Weber, M. Marinak, S. Wunsch, C. Garsi, A. Robinson, M. Andrews, P. Ramaprabhu, A.C. Calder, B. Fryxell, J. Bielle, L. Dursi, P. MacNiece, K. Olson, P. Ricker, R. Rosner, F. Timmes, H. Tubo, Y.-N. Young, M. Zingale, A comparative study of the turbulent Rayleigh–Taylor instability using high-resolution three-dimensional numerical simulations: the Alpha-Group collaboration, Phys. Fluids 16 (2004) 1668–1693.
[30] R. Courant, K. Friedrichs, Supersonic Flow and Shock Waves, Springer-Verlag, New York, 1967.
[31] A. Azevedo, D. Marchesin, Multiple viscous solutions for systems of conservation laws, Trans. Amer. Math. Soc. 347 (1995) 3061–3078.